Scanning Electron Microscopy

Volume 3
Number 1 *3rd Pfefferkorn Conference*

Article 26

1984

Energy Selecting Electron Microscopy

F. P. Ottensmeyer
Ontario Cancer Institute

Electron Optical Systems (pp. 245-251)
SEM Inc., AMF O'Hare (Chicago), IL 60666-0507, U.S.A.

0-931288-34-7/84$1.00+.05

ENERGY SELECTING ELECTRON MICROSCOPY

F.P. Ottensmeyer

Ontario Cancer Institute
500 Sherbourne Street
Toronto, Ontario M4X 1K9
Canada
Telephone: (416) 924-0671

Abstract

One of the major improvements in transmission electron microscopy over the last years is the addition of the capability of producing images with electrons that have specific narrow energy bands out of the total spectrum of energies they possess after having passed through the specimen. Though the idea is not new, the power of this application is only beginning to be recognized. Most simply, selection of elastically scattered electrons permits increased contrast in high resolution images in bright field, dark field, and diffraction. The use of combined elastic and inelastic signals adds entirely new contrast mechanisms, partially independent of thickness, partly Z-related. Finally, selection of element specific inelastic events permits elemental mapping with spatial resolutions of 0.3 - 0.5 nm and detection sensitivities of about 30 to 50 atoms. Consideration of resolution, sensitivity, image points of analysis and acquisition time leads to a combined improvement of about 10^{13} times over X-ray microanalysis.

Key words: microanalysis, electron energy filter, elastic scatter, sector magnet, imaging filter, transmission electron microscopy, electron diffraction.

Introduction

Major advances in electron microscopy have come about by modifications of the basic design of the instrument which were simple to adapt: the introduction of the stigmator, or the double condenser system; by changes in technique that were easy to implement: sectioning of tissues or staining for contrast; or on the other hand by radical alterations which were so dramatic in effect that the effort in adaptation both by the manufacturer and the user was more than compensated by the result: the introduction of the scanning transmission electron microscope.

One area which has been puzzlingly neglected is the addition of energy selection to the imaging capabilities of the electron microscope. Certainly the problem of chromatic aberration in the image of a specimen has been recognized, with much effort being expended to design round lenses that would not limit resolution due to the natural energy spread of the electron gun. The secondary effect of energy spread due to inelastic scatter of electrons within the specimen being imaged has been less emphasized, although a number of multipole lenses have been designed to correct chromatic aberrations for at least part of the change in energy encountered in the specimen (16). However, the complexity of these systems has to the present prevented their proliferation in non-experimental situations.

An alternative to correction of lenses is the filtering of the energies in the electron beam after it has passed through the specimen. In addition to obviating chromatic aberrations, such an approach has the added benefit of being able to extract more information from the beam on fundamental electron scattering phenomena as well as on the chemistry of the specimen via characteristic interactions.

Energy selecting systems

Probe forming

A number of such energy selecting electron microscopes have been built experimentally. The simplest in principle is the extension of the use of a probe forming system equipped with an electron spectrometer such as an attached sector magnet. Scanning of the probe while selecting a specific energy band in the electron energy

spectrum permits energy selected microscopy for bright field elastic images and images with a selected energy loss under axial illumination. Pure elastic dark field images are not possible with present systems, though due to a partial angular separation of elastic and inelastic scatter, a reasonable approximation to elastic dark field can be obtained for thin specimens using the signal from the annular aperture detector in the STEM. High resolution (0.5 nm) elemental maps using probe forming systems are only possible in STEM's equipped with field emission guns. Nevertheless, even for such systems the total beam current in the small probe is still so feeble that mapping of a small area of, say, 128 x 128 picture points still requires about 15 minutes (15). This is in sharp contrast to the use of vastly more efficacious parallel filtering systems below.

Line scanning

An approach to improvement over a point by point image analysis was the passage of an entire image line simultaneously through an electrostatic filter lens (20,25). Information in the image line was spread out in energy at right angles to the line; and a long slit could select the desired energy band. Scanning of the image a line at a time over an entrance slit followed by simultaneous "unscanning" of the energy selected line emerging from the exit slit built up an energy selected micrograph.

Two-dimensional filtration

However, the most efficacious approach is to filter an entire two-dimensional image simultaneously. If elastic bright field or dark field images only were desired, then a threshold filter, a passage of electrons through a grid that presented a voltage barrier which could only be surmounted by electrons that had not lost energy, would be sufficient. Much more versatile is an imaging spectrometer. We have found that a development of a prism-mirror-prism system as an integrated part of a fixed beam electron microscope (8,14,22) not only does not deteriorate the performance of the microscope, but instead provides superior images to the unmodified microscope in all modes of operation, in addition to offering the unique features of energy analysis, microanalysis and elemental mapping that only an imaging energy selecting system can provide. Similar systems have been built (13), while other devices have included a system of crossed electric and magnetic fields (10), as well as two all-magnetic imaging electron energy filters incorporating sector magnets (18,26). The latter eliminate the requirement for an electrostatic mirror operating at the high tension of the electron gun, and have manifold more possibilities of introducing corrective elements. To date however, they have not performed as well in imaging as the mirror-prism system, possibly due to their slightly younger state of development or the difficulties arising from their greater structural complexity.

Our system is shown in principle in Fig. 1. The system is installed as an integral permanent component in the column of a transmission microscope (Siemens Elmiskop 102) above the projector lens. As such it must perform two functions. First, it must act like a spectrometer. This is not too difficult, since any reasonable sector magnet does this superbly. Second and much more crucially, it must act like a lens. Since the system is neither centro-symmetric nor round as are most familiar lenses, it is a priori not at all clear that it should do so. Nevertheless, properly aligned, it does. The symmetry it posesses about the axis of the mirror cancels many even of the second order aberrations in the image, while its position in the microscope reduces remaining errors by prior magnification of the image to such a degree that at any final magnification such errors are smaller than the electron impact size in the photographic material that records the image.

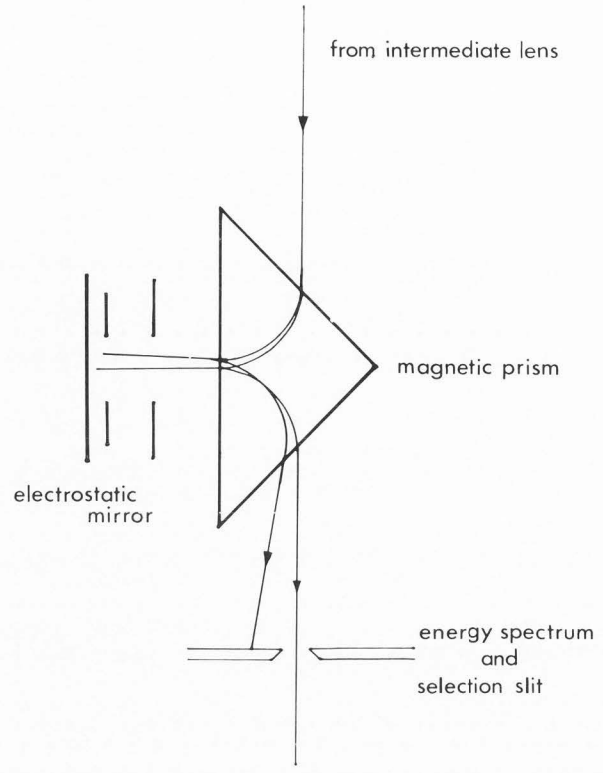

Figure 1. Schematic of imaging energy filter. The electron energy spectrum occurs at the electrostatic mirror and, with twice the dispersion, at the level of the selecting slit. An achromatic image is formed at the cross-over of the beams on the second pass through the prism.

Application

Fig. 2 shows the 0.204 nm lattice lines of gold taken through the filter as an indication that the performance of the original microscope is not deteriorated. On the contrary, the opposite is true, since the normal operating mode of this microscope uses only unscattered or elastically scattered electrons. The effect in every case is a small or large increase in contrast (Fig. 3), depending on the size of the inelastic contribution to the conventional image. Such a conventional image can still be produced by retracting the energy selecting slits (Fig. 1,

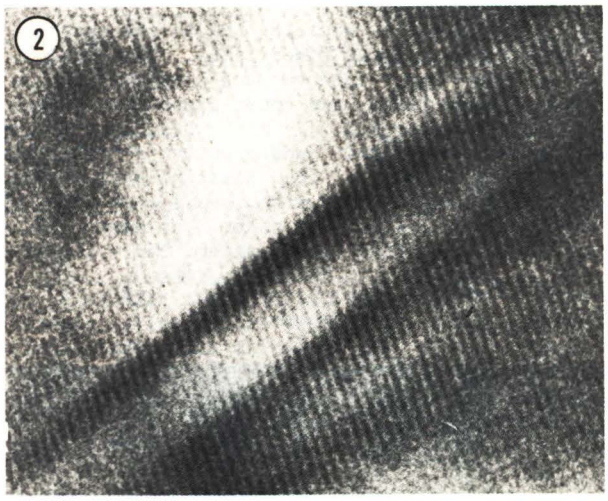

Figure 2. Energy filtered elastic image of a single crystal gold foil showing 0.204 nm lattice lines.

Fig. 3a). The advantage of energy selection is perhaps more important in low contrast unstained material and thicker specimens such as used in enzyme cytochemistry or X-ray microanalysis. Again in bright field the elastic image provides somewhat greater contrast (Fig. 4a,4b), but for such thin unstained specimens as this section the elastic dark field mode (Fig. 4c) gives the expected huge increase in contrast (24), though now without any deleterious effects of chromatic aberration that occurs in the conventional dark field image.

Of course, being a compleat instrument, the energy selecting electron microscope permits diffraction mode operation like a normal microscope, with the additional choice of total, elastic, total inelastic or energy selected options (Fig. 5). The example also demonstrates the effect of modifying the effective acceptance angle of the filter by means of the pre-spectrometer lenses. Though the spectrometer itself has an acceptance half-angle of about 15 mradians, the half-angle passed by the prism referred to the specimen in these diffraction patterns is easily about 100 mradians. The analysis of fundamental scattering phenomena in electron-matter interactions becomes not only possible with such a device, but easy.

Recently interest has revived in an imaging mode using elastic dark field images divided point by point by the corresponding energy loss signal (6). This was first demonstrated in the STEM (7,9), but is of course also possible in a fixed beam energy selecting microscope (23). Simple theory indicates that the combined signal is proportional to the atomic number of the constituent atoms in the specimen and independent of the thickness (19). However, more careful consideration indicates a partial thickness dependence (12), a strong effect of unsharp masking due to non-local scatter in the inelastic signal, and specific variations due to the presence of ionization edges which tend to reduce the signal of the corresponding atomic element (23). The total effect is interesting, and may

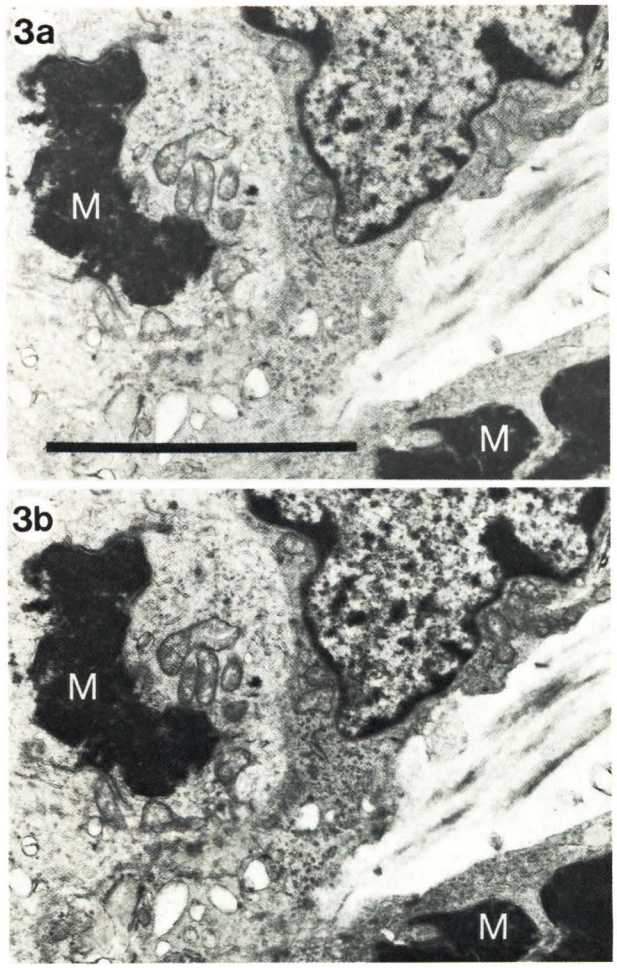

Figure 3. Section through a malignant testicular tumor showing two of many mitotic figures (M) of rapidly dividing cells. The specimen is a standard pathological tissue preparation, glutaraldehyde fixed, post-fixed with osmium tetroxide, stained with uranyl acetate and lead citrate. (a) Bright field electron micrograph using all energies. (b) Elastic bright field image. Both images were printed identically on soft (zero) paper. The increase in contrast in (b) is due to removal of inelastically scattered electrons. Bar = 5 μm.

be useful; but it must be more thoroughly investigated in order to be understood more fully.

However, the most emphasized characteristic of energy selected microscopy is elemental microanalysis. Certainly, incorporating an electron spectrometer, the microscope provides point or area analysis (Fig. 6). But more important, pairs of energy selected images (ESI, electron spectroscopic images) taken at energies such as the hashed areas in Fig. 6, one above a specific atomic ionization edge, another just below this edge in energy, immediately provide a qualitative indication of the presence and distribution of the specific corresponding atom. This is demonstrated for titanium and copper in the extraction replica of a low alloy steel in Fig. 7, and for phosphorus in the section of a

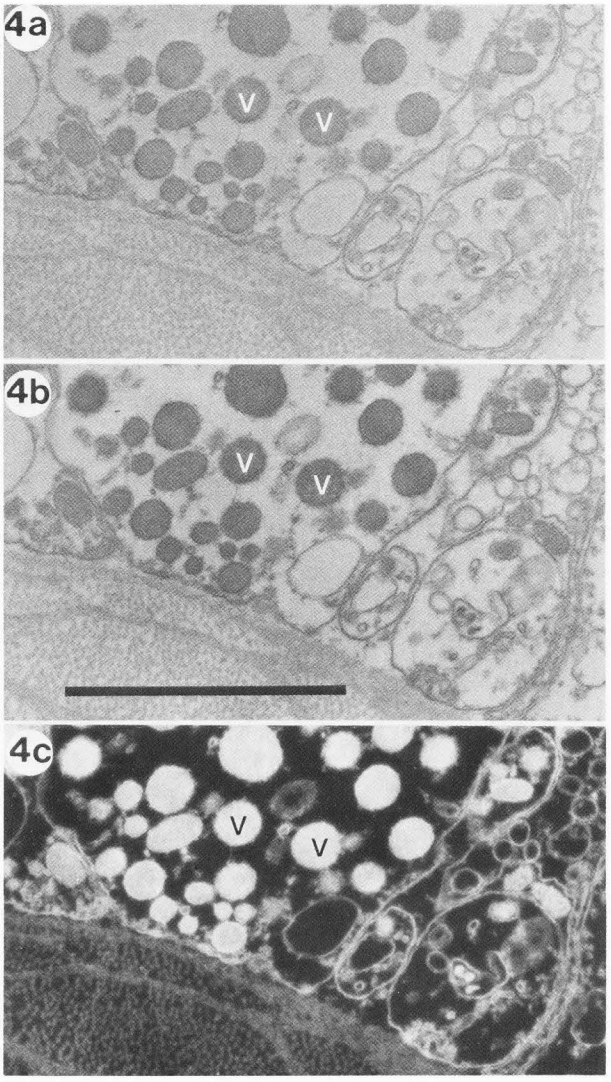

Figure 4. Secretory vesicles (v) in the tegument of the lobster Homarus americanus. The section, dark gray by interference colours, is glutaraldehyde fixed and post-fixed with osmium tetroxide, unstained. (a) Bright field micrograph using all energies. (b) Elastic bright field image. (c) Elastic dark field image. The bright field micrographs were printed identically on soft (#1) paper, the dark field image on still softer (zero) paper. Bar = 1.0 μm.

Figure 5. Diffraction pattern of a thin foil of aluminum, using all energies (total), elastic electrons (el), all inelastic electrons (inel) and various selected energy losses (∓6 eV) as indicated. A band of intensity corresponding to the Bethe ridge (11) moves out from the centre with increasing selected energy losses (arrows).

Figure 6. Electron energy spectrum of an extracellular deposit from an osteoblast (bone-forming cell) in culture (22). The ionization edges occurring in this specimen are identified. The two hashed areas indicate the energy regions with which energy selected images must be taken as a minimum requirement (see text) for elemental mapping of calcium.

Figure 7. Energy selected images of a carbon extraction replica containing precipitates from the surface of a low alloy steel. (a) Elastic bright field image showing precipitates of various sizes and shapes. (b) and (c) A selected area from (a) taken below and above the L-shell ionization edge of titanium. The local increases in brightness in (c) compared to (b) indicate that the larger rectangular precipitates (arrows) contain Ti. (d) and (e) The same area taken with energies below and above the L-shell ionization of copper. The local increases in intensities in (e) compared to (d) indicate the presence of Cu in the small precipitates. The larger Ti-containing precipitates are unchanged in intensity relative to the background, indicating an absence of Cu in these. Micrographs (b) to (e) were printed identically on soft (zero grade) paper. Bar = 1.0 μm.

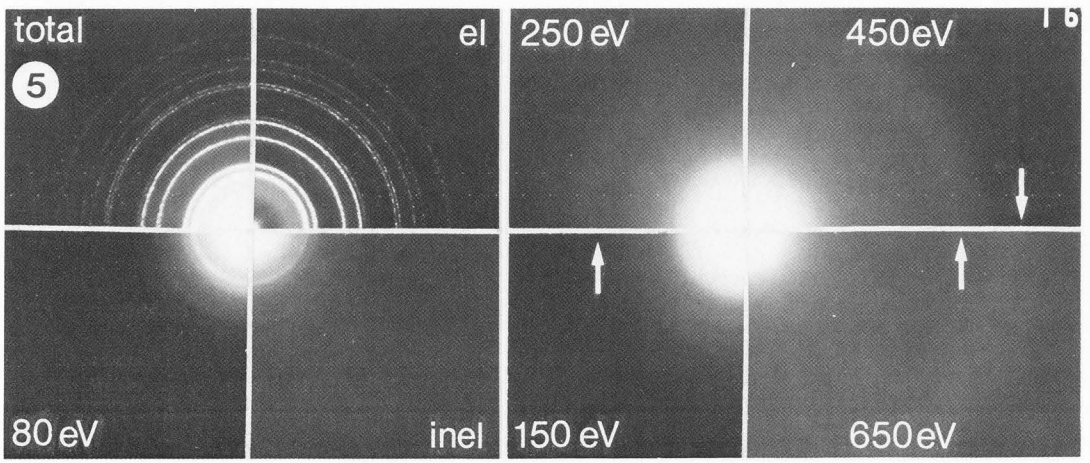

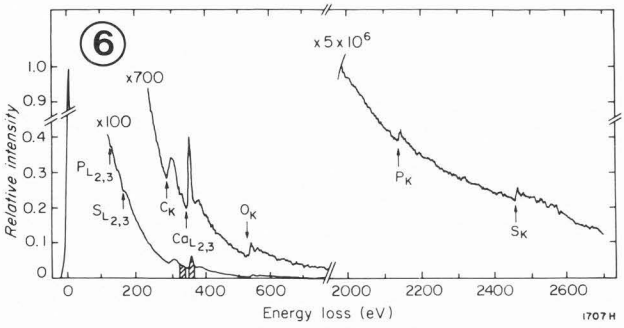

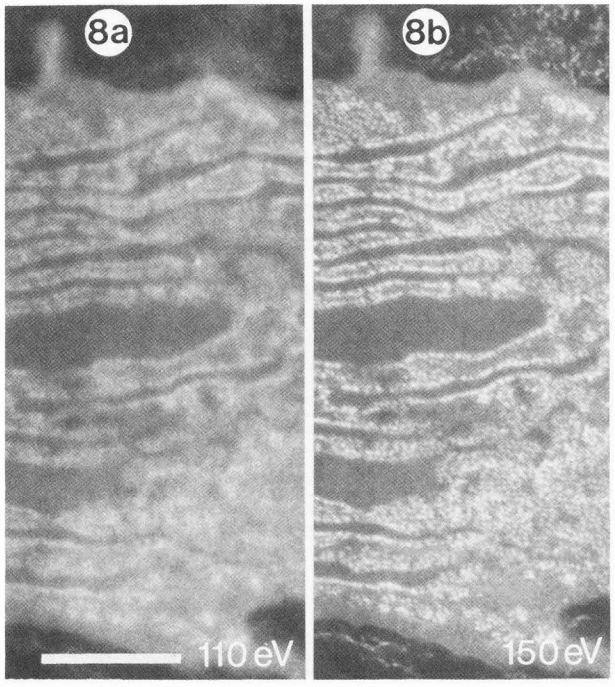

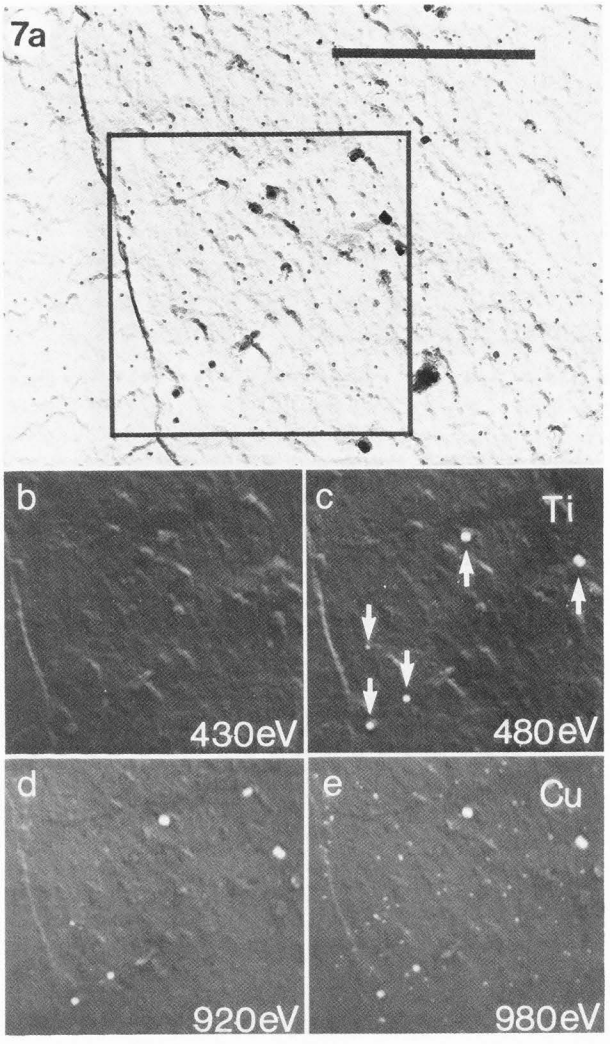

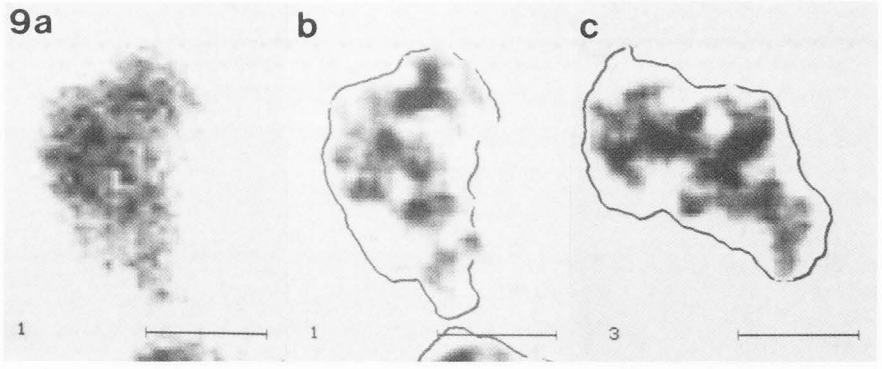

Figure 8. Energy selected micrographs of an unstained section through a chondrocyte in the developing cartilage of the mouse, taken with energies below (a) and above (b) the phosphorus L-shell ionization edge. The increase in local brightness in (b) indicates the presence of P predominantly in the ribosomes of the rough surfaced endoplasmic reticulum. Bar = 0.5 μm.

Figure 9. Phosphorus map within 20 nm long E. coli 30S ribosomal subunits. (a) Energy selected image at 150 eV, just above the P L-shell ionization edge at 132 eV. Phosphorus distribution within the particle in (a) obtained by computer-assisted subtraction of the image in (a) minus its corresponding image taken at 110 eV, below the P L-edge. The contour of the particle in (a) is shown for reference (c). Phosphorus map within another 30S particle at a different orientation. Bar = 8.0 nm.

chondrocyte in Fig. 8. In each case the extraordinary local increase in intensity or contrast relative to the surrounding background for the image above the ionization edge, compared to the image below the edge in energy, signals the presence of the corresponding atomic element. Pure elemental maps can be obtained over entire micrographs by suitable normalization of the two images, alignment and photographic subtraction (22), or by densitometry and computer-assisted image processing of smaller regions selected a posteriori in the image. The latter process was carried out for the phosphorus map within 20 nm long 30S ribosomal subunits in Fig. 9 (17).

Any element from Z = 1 to Z = 92 can be examined by the technique, using low energy signals of the K-shell ionizations for low atomic number elements and L-, M-, N-, and O-shells for higher Z atoms. While we have not tried to be exhaustive, our normal work has so far included the analysis and mapping of B, C, O, N, F, Mg, Al, Si, P, S, Ca, Ti, Fe, Cu, Zn, Ag, W, and U. Applications have ranged from the investigation of Al and W in semi-conductors, P- and Si-containing inclusions in reactor tube cladding, Si deposits in plant fungal infections (21), Ca, S, and P distributions in normal and diseased developing cartilage and bone (2,3), to high resolution maps of the phosphorus distribution within ribosomal particles (6,17) and within nucleosomes, the 10 nm subunits of the fine structure of chromosomes(4,5).

At present the local concentration of the elements examined has been rather high (e.g. 3 M phophorus within the double helix of DNA) even though the absolute amounts detected are only a few tens of atoms. Thus the use of a single pair of images bracketing the specific ionization edge has been sufficient to delineate and quantify a specific element. For a more accurate quantitative approach two or more images displaced in energy below the selected ionization edge could be used to extrapolate the background signal under the edge more precisely. But a compromise here is necessary, since preceding ionization edges and their extended fine structure (Fig. 6) can strongly influence such an extrapolation. Moreover, for a reliable extrapolation even without such complications some averaging over many pixels over and around the point of interest is necessary to overcome noise fluctuations in individual pixels, that are incurred by low electron exposures used to spare sensitive specimens. This practical limitation unfortunately negates to some extent the advantage of a scanning approach in which ideally such an extrapolation could be performed by curve-fitting to a continuous spectrum at every point.

Electron spectroscopic images, which contain as many as 50 million picture points at the resolution of the photographic plate, are taken in a few seconds in a fixed beam transmission electron microscope, compared to a 15 minute exposure for as few as 128 x 128 pixels in even a dedicated STEM with sector magnet spectrometer and field emission gun (15). This major difference is due to the fact that in spite of the high directed brightness of the field emission gun, the total current in the beam at the specimen is of the order of 10^{-9} A compared to 10^{-6} A for the thermionic gun. Operationally the beam in the STEM has to be apertured and focused into a small spot to achieve high spatial resolution in scanning. In contrast the beam of the thermionic gun in a fixed beam microscope does not have to be focused, but indeed has to be spread over the image for most applications we have encountered so far. Effectively, for elemental mapping via an imaging filter the probe size in the fixed beam microscope is not the beam size, but the size of the wave packet of every individual electron in that beam.

Ideally, for elemental mapping in an energy selecting microscope with imaging filter the shortest exposure times could be obtained by matching the minimum possible spot size of the fully condensed beam to the field of view at any magnification. Since for magnifications commonly used in biology this would mean minimum spot sizes as large as several tens of microns, this would be a reversal in thought in electron gun design, which over the last years has striven for small spot sizes.

Conclusion

An energy selecting electron microscope based on an integrated imaging electron spectrometer in a fixed beam microscope offers unhindered normal operational functions with improvement in contrast, coherence and resolution in the image. Pure elastic bright field, dark field and diffraction become standard operation modes, obviating problems due to chromatic aberrations in the image. In addition energy selection in the electron energy loss spectrum provides fundamental data on dispersion of electrons with energy loss, as well as producing high contrast images for thin specimens, that form the basis for elemental mapping with spatial resolutions as good as 0.3 to 0.5 nm and sensitivities of detection in analysis as low as 30 to 50 atoms (1,4). Energy loss spectra over selected areas, recorded in parallel or sequentially, are part of the normal capabilities. Our own microscope (Siemens 102) is not equipped with a probe forming lens, making very small spot analysis via spectra impossible. In more modern instruments this is no longer a limitation. In addition, since the device disturbs neither the specimen area nor the column exit, any adaptations such as goniometers, cooling stages, X-ray microanalysis (as complementary technique of microanalysis for thick specimens), TV cameras etc. are entirely compatible with the design.

Acknowledgements

Thanks are due to H. Hashimoto, W. Rothenburger, A.L. Arsenault, G.C. Weatherly and A.P. Korn for the specimens in Figs. 2, 3, 4 and 8, 7, and 9 respectively. The work was supported by the Ontario Cancer Treatment and Research Foundation, the National Cancer Institute of Canada and grant MT-6337 from the Medical Research Council of Canada.

References

1. Adamson-Sharpe, K.M., Ottensmeyer, F.P. (1981). Spatial resolution and detection sensitivity in microanalysis by electron energy loss selected imaging. J. Microsc. 122:309-314.

2. Arsenault, A.L., Ottensmeyer, F.P. (1983). Quantitative spatial distribution of calcium, phosphorus and sulfur in calcifying epiphysis by high resolution spectroscopic imaging. Proc. Natl. Acad. Sci., U.S.A. 80:1322-1326.

3. Arsenault, A.L., Ottensmeyer, F.P., (1984). Visualization of early intramembranous ossification by electron microscopic and electron spectroscopic imaging. J. Cell. Biol. 98:911-921.

4. Bazett-Jones, D.P., Ottensmeyer, F.P. (1981). Phosphorus distribution in the nucleosome. Science 211:169-170.

5. Bazett-Jones, D.P., Ottensmeyer, F.P. (1982). DNA organization in nucleosomes. Can. J. Biochem. 60:364-370.

6. Boublik, M., Oostergetel, G.T., Frankland, B., Ottensmeyer, F.P. (1984). Topographical mapping of ribosomal RNAs in situ by electron spectroscopic imaging. Proc. 42nd Ann. Meet. EMSA, G.W. Bailey (ed.), San Francisco Press, pp. 690-691.

7. Carlemalm, E., Kellenberger, E. (1982). The reproducible observation of unstained embedded cellular material in thin sections: visualization of an integral membrane protein by a new mode of imaging for STEM. Europ. Molec. Biol. Org. J. 1:63-67.

8. Castaing, R., Henry, L. (1962). Filtrage magnetique des vitesses en microscopie electronique. C.R. Acad. Sci., Paris B255:76-78.

9. Crewe, A.V., Wall, J., Langmore, J. (1970). Visibility of single atoms. Science 168:1338-1340.

10. Curtis, G.H., Silcox, J. (1971). A Wien filter for use as an analyser with an electron microscope. Rev. Sci. Instrum. 42:630-637.

11. Egerton, R.F. (1979). K-shell ionization cross-sections for use in microanalysis. Ultramicroscopy 4:169-179.

12. Egerton, R.F. (1982). Thickness dependence of the STEM ratio image. Ultramicroscopy 10:297-299.

13. Egerton, R.F., Philip, J.G., Turner, P.S., Whelan, M.J. (1975). Modification of a transmission microscope to give energy loss spectra and energy selected images and diffraction patterns. J. Phys. E8:1033-1037.

14. Henkelman, R.M., Ottensmeyer, F.P. (1974). An energy filter for biological electron microscopy. J. Microscopy 102:79-94.

15. Jeanguillaume, C., Tence, N., Trebbia, P, Colliex, C. (1983). Electron energy loss chemical mapping of low Z elements in biological sections. Scanning Electron Microsc. 1983; II:745-756.

16. Koops, H. (1978). Aberration correction in electron microscopy. In: Electron Microscopy 1978. Vol. III State of the Art. Proc. 9th Intnl. Congr. Electron Micr., J.M. Sturgess (ed.), Microsc. Soc. Canada (publ.), Toronto; pp. 185-196.

17. Korn, A.P., Spitnik-Elson, P., Elson, D., Ottensmeyer, F.P. (1983). Specific visualization of ribosomal RNA in the intact ribosome by electron spectroscopic imaging. Eur. J. Biochem. 31:334-340.

18. Krahl, D., Hermann, K.-H., Kunath, W. (1978). Electron optical experiments with a magnetic imaging filter. In: Electron microscopy 1978 (Proc. 9th Intnl. Cong., ed. J.M. Sturgess; Microscopical Soc. Canada, Toronto). Vol. 1, pp. 42-43.

19. Lenz, F. (1952). Zur Streuung mittelschneller Elektronen in kleinste Winkel. Z. Naturforsch. 9a:185-204.

20. Moellenstedt, G. (1949). The electrostatic lens as a velocity analyser of high resolving power. Optik 5:499-517.

21. Ottensmeyer, F.P. (1982). Scattered electrons in microscopy and microanalysis. Science 215:461-466.

22. Ottensmeyer, F.P., Andrew, J.W. (1980). High resolution microanalysis of biological specimens by electron energy loss spectroscopy and electron spectroscopic imaging. J. Ultrastruct. Res. 72:336-348.

23. Ottensmeyer, F.P., Arsenault, A.L. (1983). Electron spectroscopic imaging and Z-contrast in tissue sections. Scanning Electron Microsc. 1983;IV:1867-1875.

24. Ottensmeyer, F.P., Pear, M. (1975). Contrast in unstained sections: a comparison of bright and dark field electron microscopy. J. Ultrastruct. Res. 51:253-260.

25. Watanabe, H., Uyeda, R. (1962). Energy selecting electron microscope. J. Phys. Soc. Japan 17:569.

26. Zanchi, G., Sevely, J., Jouffrey, B. (1977). An energy filter for high voltage electron microscopy. J. Microsc. Spectrosc. Electron. 2:95-104.